ELEMENTA
Science of the Anthropocene

Variability analyses, site characterization, and regional [OH] estimates using trace gas measurements from the NOAA Global Greenhouse Gas Reference Network

Jan Pollmann[1,2] • Detlev Helmig[1*] • Daniel Liptzin[1] • Chelsea R. Thompson[1] • Jacques Hueber[1] • Pieter P. Tans[3] • Jos Lelieveld[2]

[1]Institute of Arctic and Alpine Research (INSTAAR), Boulder, Colorado, United States
[2]Max Planck Institute for Chemistry, Mainz, Germany
[3]Earth System Research Laboratory, National Oceanic and Atmospheric Administration (NOAA/ESRL), Boulder, Colorado, United States
*Detlev.Helmig@colorado.edu

Abstract

Trace gas measurements from whole air samples collected weekly into glass flasks at background monitoring sites within the NOAA Global Greenhouse Gas Reference Network program (with most of the sites also being World Meteorological Organization (WMO) Global Atmospheric Watch (GAW) stations) were used to investigate the variability-lifetime relationship for site characterization and to estimate regional and seasonal OH concentrations. Chemical species considered include the atmospheric trace gases CO, H_2, and CH_4, as well as the non-methane hydrocarbons (NMHC) ethane (C_2H_6), propane (C_3H_8), *i*-butane (*i*-C_4H_{10}), and *n*-butane (*n*-C_4H_{10}). The correlation between atmospheric variability and lifetime was applied on a global scale spanning 42 sites with observations covering a period of 5 years. More than 50,000 individual flask measurement results were included in this analysis, making this the most extensive study of the variability-lifetime relationship to date. Regression variables calculated from the variability-lifetime relationship were used to assess the "remoteness" of sampling sites and to estimate the effect of local pollution on the measured distribution of atmospheric trace gases. It was found that this relationship yields reasonable results for description of the site remoteness and local pollution influences. Comparisons of seasonal calculated OH concentrations ([OH]) from the variability-lifetime relationships with six direct station measurements yielded variable agreement, with deviations ranging from ~20% to a factor of ~2–3 for locations where [OH] monitoring results had been reported. [OH] calculated from the variability-lifetime relationships was also compared to outputs from a global atmospheric model. Resutls were highly variable, with approximately half of the sites yielding agreement to within a factor of 2–3, while others showed deviations of up to an order of magnitude, especially during winter.

Managing Editor-in-Chief
Michael E. Chang,
Georgia Institute of Technology

Guest Editor
Frank Flocke,
National Center for Atmospheric Research

Knowledge Domain
Atmospheric Science

Article Type
Research Article

Part of an *Elementa* Special Feature
Reactive Gases in the Global Atmosphere

Received: February 11, 2016
Accepted: August 22, 2016
Published: October 28, 2016

1. Introduction

The relationship between the variability in mole fraction and the lifetime of long-lived trace gases in the atmosphere was first described by Junge (1974). An inverse relationship was observed between the relative standard deviation of the mole fraction of trace gases and its atmospheric lifetime. In essence, this relationship signifies that the most reactive trace gases exhibit the greatest variability. This approach was later refined and extended to shorter-lived non-methane hydrocarbons (NMHC) (Jobson et al., 1998, 1999) by employing the standard deviation of the natural logarithm of the gases' mole fraction rather than the relative standard deviation. This simplifies the mathematical relationship because the log-transformed molar ratio of a hydrocarbon decreases linearly as a function of its oxidation rate.

The variability-lifetime relationship as proposed by Jobson et al. (1998) is described by Equation 1:

$$s_{\ln X} = A\ \tau^{-b} \quad (1)$$

This equation has been evaluated and applied multiple times in previous literature based on a variety of different atmospheric trace gases and time scales (Ehhalt et al., 1998; Jobson et al., 1998, 1999; Williams et al., 2000; Karl et al., 2001; Williams et al., 2001, 2002; Karl et al., 2003a; Karl and Guenther, 2004). Short duration studies with high frequency data of short-lived compounds (e.g. Karl et al., 2003b; Karl and Guenther, 2004) are useful for examining local sources and sinks at short time scales and with regional footprints. Measurement sites that are impacted by local emissions are not suitable for an analysis of synoptic concentration changes as the variability of the gases becomes dependent upon emission source variability rather than atmospheric loss rate, resulting in little or no dependence on lifetime. The lifetime-variability relationship has been described in detail in the references cited above; therefore, only a brief explanation of the approach is given here. $s_{\ln X}$ is the standard deviation of the natural logarithm of the mole fraction of all measurement values; A is a proportionality factor (see further below); b is an indicator of the source-receptor distance with values between 0 and 1; and τ is the atmospheric lifetime of the investigated species. This relationship is expected to be valid for all atmospheric trace gases when the results of the natural logarithm of the observed mole fractions of a particular atmospheric species follows a Gaussian distribution. Data sets with a significant fraction of measurements at or below the detection limit do not follow a Gaussian distribution and will deviate from the variability lifetime relationship (Jobson et al., 1998, 1999).

The b-value describes the influence of emission sources and thus can be used to characterize the "remoteness" of a measurement site. A low b-value, i.e. $b < 0.3$, indicates influence from nearby emission sources and non-remote conditions. b-values of 0.5 or higher have been found for samples from remote surface stations, while $b \approx 1$ was reported for stratospheric sample sets (Ehhalt et al., 1998; Jobson et al., 1999; Williams et al., 2001).

In contrast to the relatively well understood interpretation of the b-value, explanation of the A-value has been less satisfactory (Jobson et al., 1998). Previous studies interpreted this factor as an indicator for the age range of the sampled air mass (Karl et al., 2001). These authors argue that high values would indicate a diverse age range (i.e., aged air as well as recent input of pollution was sampled), whereas smaller values would be a sign for a more homogeneous age range of the sampled air masses. Consequently, high A-values are expected for stations that are occasionally affected by nearby sources. Highly variable photochemical conditions might also result in elevated A-values. According to this interpretation, samples from tropical regions, and stratospheric datasets, where conditions are more uniform, would exhibit low A-values, representing a more homogenous source distribution and photochemical and meteorological conditions.

Globally, oxidation of atmospheric hydrocarbons is primarily initiated by the OH radical; thus, the variability-lifetime relationship is directly related to the OH concentration ([OH]), making it possible to estimate regional [OH] from NMHC observations. Several studies have used the atmospheric variability-lifetime relationship to estimate the regional [OH] that an air mass was exposed to before reaching a particular measurement station (Ehhalt et al., 1998; Jobson et al., 1999; Williams et al., 2000; Karl et al., 2001). These results were within 50% or better of model calculations and direct measurements of [OH] (Karl et al., 2001; Williams et al., 2001; Bartenbach et al., 2007). This method relies on the knowledge of the atmospheric lifetime and the local concentration of a trace gas whose atmospheric decay is not dependent on OH oxidation, such as of chlorofluorocarbons (CFC), gases that undergophotolysis (e.g., acetone), radioactive decay (e.g. radon), or as will be discussed in this paper, H_2 and SF_6. The lifetime of this species is kept fixed while the lifetimes of the other compounds are varied to solve for the best fit of equation 1. The [OH] associated with the best-fit solution is thought to represent the average [OH] an air mass experienced during transport towards the measurement site.

Variability analysis may be a simple way to characterize sampling locations and extract information for the understanding of the atmosphere from already available data at a fraction of the resources needed to deploy a multitude of field instrumentation for new observations. Here we aim to evaluate the applicability of this tool for the assessment of background conditions, impacts from local pollution, and estimation of regional [OH] using the most extensive data set to date in terms of number of sites and number of samples considered.

2. Experiment

2.1. NMHC and trace gas measurements

The NMHC and other trace gas species measurements used for this analysis are from samples collected by the US National Oceanic and Atmospheric Administration (NOAA) Global Greenhouse Gas Reference Network (GGGRN) at mostly regional and global sites (see Figure 1 for a map of site locations and Table 1

Table 1. NOAA Global Greenhouse Gas Reference Network sites used in this analysis, sorted by latitude, with three letter code, location, altitude, and the mean *A* and *b* values for each season for the years 2004–2011

Station	Code	GAW Status	Latitude	Longitude	Altitude (m asl)	*A*		*b*	
						Jun-Aug	Dec-Feb	Jun-Aug	Dec-Feb
Alert, Canada	ALT	Global	82.45	-62.52	210	5.16	1.62	0.72	0.61
Ny Alesund, Norway	ZEP	Global	78.90	11.88	1320	5.33	2.36	0.80	0.66
Summit, Greenland	SUM	Regional	72.58	-38.48	3238	3.44	2.01	0.78	0.61
Barrow, AK, USA	BRW	Global	71.32	-156.6	11	4.65	1.72	0.74	0.59
Pallas, Finland	PAL	Global	67.97	24.12	560	1.09	2.29	0.56	0.66
Vestmannaeyjar, Iceland	ICE	Regional	63.34	-20.29	127	4.68	1.31	0.82	0.62
Baltic Sea, Poland	BAL	Regional	55.35	17.22	28	2.00	0.67	0.68	0.44
Cold Bay, AK, USA	CBA	Regional	55.12	162.42	25	4.40	2.09	0.75	0.67
Lac La Biche, Alberta, Canada	LLB	Regional	54.95	-112.45	540	1.53	0.53	0.58	0.33
Mace Head, Ireland	MHD	Global	53.33	-9.9	25	1.49	2.38	0.56	0.72
Shemya, AK, USA	SHM	Regional	52.72	174.1	40	3.29	1.54	0.75	0.66
Ochsenkopf, Germany	OXK	Contrib. Reg.	50.06	11.8	1356	0.74	0.55	0.48	0.41
Hohenpeissenberg, Germany	HPB	Global	47.8	11.01	990	0.48	0.49	0.48	0.42
Park Falls, WI, USA	LEF	Regional	45.93	-90.27	868	3.70	1.69	0.72	0.59
Argyle, ME, USA	AMT	Contrib. Reg.	45.03	-68.88	157	2.64	1.90	0.62	0.62
Black Sea, Romania	BSC	Regional	44.17	28.68	3	1.96	1.60	0.53	0.44
Trinidad Head, CA, USA	THD	Global	41.05	-124.15	107	3.21	1.68	0.72	0.57
Wendover, UT, USA	UTA	Regional	39.90	-113.72	1628	1.83	4.43	0.59	0.60
The Azores	AZR	Regional	38.77	-27.38	40	2.73	0.87	0.71	0.61
South. Great Plains, OK, USA	SGP	Contrib. Reg.	36.80	-97.5	374	0.97	0.97	0.54	0.50
Tae-ahn Peninsula, Sth Korea	TAP	Regional	36.73	126.13	20	1.48	1.86	0.49	0.51
Izana, Tennerife	IZO	Global	28.30	-16.48	2360	1.27	1.48	0.71	0.67
Midway Island	MID	Regional	28.21	-177.38	8	1.15	1.40	0.62	0.66
Assekrem, Algeria	ASK	Global	23.18	5.42	2728	1.36	1.43	0.70	0.61
Mauna Loa, HI, USA	MLO	Global	19.54	-155.58	3397	1.78	1.01	0.69	0.60
Cape Kumukahi, HI, USA	KUM	Regional	19.52	-154.82	3	3.10	2.71	0.74	0.73
High Alt. Obs. Ctr, Mexico	MEX	Non-GAW Reg.	18.98	-97.311	4464	5.24	1.83	0.81	0.67
Guam	GMI	Regional	13.43	144.78	6	1.67	1.14	0.79	0.69
Mount Kenya, Kenya	MKN	Global	-0.05	37.3	3897	0.34	2.00	0.55	0.74
Bukit Kototabang, Indonesia	BKT	Global	-0.20	100.32	864	2.61	2.30	0.70	0.70
Seychelles	SEY	Regional	-4.67	55.17	7	4.19	0.82	0.87	0.58
Ascension Island	ASC	Regional	-7.92	14.42	54	1.70	1.93	0.78	0.81
Arembepe, Bahia, Brazil	ABP	Global	-12.77	-38.17	1	1.23	0.40	0.70	0.67
American Samoa	SMO	Global	-14.24	-170.57	42	2.12	0.96	0.84	0.66
Cape Grim, Australia	CGO	Global	-40.68	144.68	94	1.23	0.82	0.78	0.75
Crozet Islands	CRZ	Regional	-46.45	51.85	120	1.32	1.11	0.77	0.75
Tierra del Fuego, Argentina	TDF	Regional	-54.87	-68.48	20	3.61	1.29	0.85	0.72
Palmer Station, Antarctica	PSA	Regional	-64.92	64	10	1.01	0.63	0.83	0.71
Syowa Station, Antarctica	SYO	Regional	-69.00	39.58	14	0.56	1.43	0.65	0.74
Halley Station, Antarctica	HBA	Global	-75.58	-26.5	33	0.71	1.57	0.73	0.81
South Pole, Antarctica	SPO	Global	-89.98	24.8	2810	1.18	1.44	0.79	0.75

doi: 10.12952/journal.elementa.000128.t001

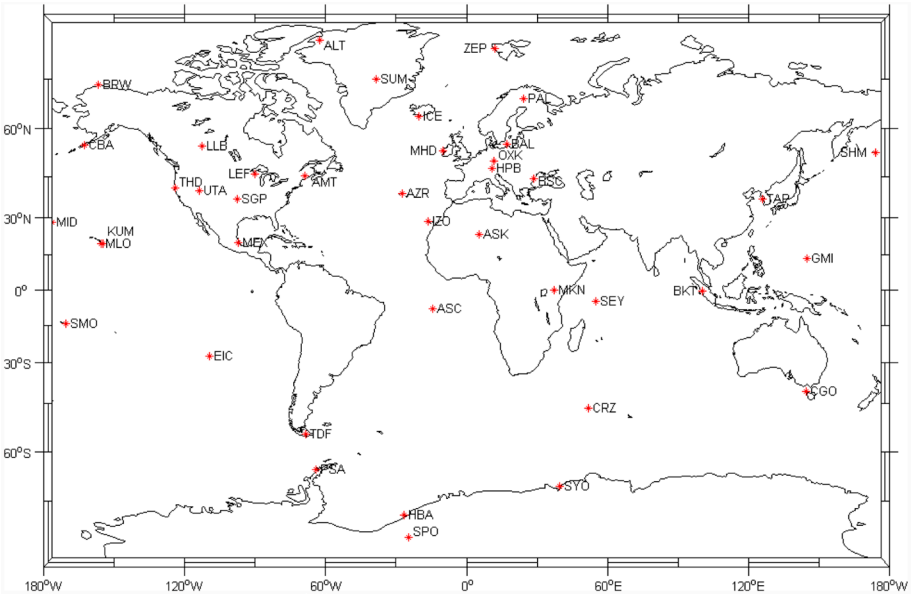

Figure 1

Locations of the 42 sites from which data were used for this study.

Station names, coordinates, elevation, and explanation of 3-letter codes used in the figure are given in Table 1.

doi: 10.12952/journal.elementa.000128.f001

for 3-letter site codes, coordinates, and elevation). This network was originally designed to study the global distribution of the greenhouse gases carbon dioxide (CO_2), methane (CH_4), nitrous oxide (N_2O), and sulfur hexafluoride (SF_6), as well as other important atmospheric trace gases such as carbon monoxide (CO), and hydrogen (H_2) (Conway et al., 1994; Dlugokencky et al., 1994), and stable oxygen and carbon isotope ratios in CO_2 and CH_4. Measurements of C_2-C_5 NMHC were added to this suite of analyses in spring 2005. The network currently consists of ~60 surface air sampling stations. Data are made available to the public through the NOAA Greenhouse Gas Reference Network (NOAA, 2016a) and the World Data Centre for Greenhouse Gases (WDCGG, 2016). NMHC covering the 2004–2011 time period were analyzed in a subset of 42 sites at the time of this study.

Details about the technical aspects and calibration procedures for the gas chromatography (GC) NMHC measurements from the network flasks have been provided in previous publications (Pollmann et al., 2006; Tanner et al., 2006; Pollmann et al., 2008; Pozzer et al., 2010; Helmig et al., 2014). In short, air was collected into a pair of 2.5 l glass flasks weekly at each sampling station and sent to Boulder, Colorado, for analysis. After analysis of greenhouse gases and inorganic trace gases (CO_2, CO, CH_4, SF_6, N_2O, H_2), as well as the carbon and oxygen isotopes in CO_2 and CH_4, the remaining sample air in the flasks was analyzed for C_2 to C_5 NMHC at the Institute or Arctic and Alpine Research (INSTAAR), University of Colorado, Boulder. The VOC monitoring is under the umbrella of the World Meteorological Organization (WMO) Global Atmospheric Watch (GAW) for Volatile Organic Compounds (VOC) (Helmig et al., 2009; Schultz et al., 2015). Within this framework the INSTAAR lab was audited by the World Calibration Center (WCC-VOC, 2016) for VOC in 2009 and 2011 and found to meet all quality control criteria set by the WMO-GAW. Approximately 5% of the measurements were filtered out when deviations between analytical results of individual flask pairs exceeded compound-specific threshold values. At one of the flask sites NMHC are also monitored in parallel with an in-situ GC instrument (Plass-Dülmer et al., 2002). Comparison of 7 years of measurements (~350 total) resulted in linear regression line slopes of 0.94–1.05 for the five NMHC considered here. More information on this program and analyses building on these data have been presented in other previous publications (Helmig et al., 2009, 2014, 2016; Pozzer et al., 2010; Emmons et al., 2014; Lawson et al., 2015).

2.2. Variability analysis

Data for a total of ten gas species, i.e., ethane, propane, *i*-butane, *n*-butane, *i*-pentane, *n*-pentane, CH_4, CO, H_2, and SF_6 were initially considered for the variability analysis. Flask data for *i*-pentane and *n*-pentane frequently fell below the detection limit, particularly for summer samples, and the remaining data set did not follow a Gaussian distribution. For these reasons, pentane data were not taken into consideration for this study.

H_2 and SF_6 data were evaluated as candidates for use as a reference point to obtain the best fit between atmospheric lifetime and variability with data for the six gases ethane, propane, *i*-butane, *n*-butane, CO, and CH_4. The atmospheric sinks of H_2 and SF_6 are not principally dependent on OH. The dominant sink for H_2 is removal by soils, accounting for ~80% or more of the total H_2 sink (Rhee et al., 2006). The remaining H_2 fraction is either removed by oxidation with OH or by transport into the stratosphere, resulting in an

overall H_2 lifetime of ~2 yrs (Hauglustaine and Ehhalt, 2002; Ehhalt and Rohrer, 2009; Yashiro et al., 2011). The soil sink is subject to seasonal changes due to the temperature dependence of microbiological activity in soils (Hauglustaine and Ehhalt, 2002). The atmospheric lifetime of SF_6 is estimated at ~3200 yrs (Forster et al., 2007).Breakdown in the stratosphere by free electrons and vacuum UV radiation above 50 km are the predominant loss processes for SF_6 (Maiss and Brenninkmeijer, 1998); however, there are significant uncertainties for the SF_6 lifetime (Reddmann et al., 2001; Laube et al., 2015). An important prerequisite for the applicability of the lifetime-variability analysis is that the variability in the data is primarily determined by the changes in atmospheric mole fraction rather than by the analytical precision error. Due to the long lifetime of SF_6, its atmospheric variability is small. Therefore, the analytical error has a relatively strong influence, despite the small uncertainty of the SF_6 analytical determination. Additionally, as noted above, the estimated lifetime of SF_6 has a large uncertainty. A variability value ($s_{\ln X}$) of $<10^{-4}$ would be expected for SF_6 by extending previously presented $s_{\ln X}$-lifetime regressions to an estimated lifetime of 3000 yr (e.g., Jobson et al., 1998, 1999). In order to accurately detect this variability, measurement precision of better than 0.001 ppt would be required, which is more than one order of magnitude smaller than the current measurement capability. Consequently, the SF_6 atmospheric variability is masked by measurement uncertainty and changes in SF_6 from the increasing trend in the atmospheric SF_6 mole fraction. For these reasons, SF_6 was excluded from the variability-lifetime analyses and H_2 was chosen instead as the reference compound.

The NMHC monitoring from network sites ramped up over the beginning years, resulting in an increasing number of available data sets between 2004 and 2011. With the filtering protocol described above and the addition of stations over time a total of 431 seasonal samples for the 42 stations were available. The number of seasonal datasets ranged from 5 to 13 across sites, but there was no latitudinal pattern in the length of the datasets. One site, Easter Island, was removed after discovering that many samples had ethane and propane concentrations that were significantly higher than background levels suggesting a local source of contamination. Only stations that follow a protocol for collection for at least one pair of flask samples per week, resulting in an average of 13 duplicate flask samples over a 3-month period, were considered for this analysis. We filtered the flask samples at each site using filtering and trend analysis tools developed by NOAA. The filtered dataset was obtained from a series of iterations that minimized residuals outside a tolerance band where the 'sigmafactor' was set to 3. More details about this data processing have been provided elsewhere (NOAA, 2016b; Helmig et al., 2016). Values lying outside the tolerance band were flagged and removed from subsequent files. We only used a data set from a particular site when there were a minimum of eight remaining duplicate samples for a season and year to minimize the risk of undersampling. During spring and fall, when solar irradiance changes relatively rapidly, NMHC show higher concentration changes and an associated larger variability. Therefore, we chose to perform this variability analysis for the times of year when atmospheric NMHC are not strongly increasing or decreasing, namely for mid-summer (Northern Hemisphere (NH) June to August, Southern Hemisphere (SH) December to February) and mid-winter (NH December to February, SH June to August). For a test of the robustness of the variability analysis, we chose data from a site, e.g., Ascension Island, for which weekly data were available, and performed calculations on a randomly subsampled group of ~ 50% of the data. Results for the subsets were within <5% of the results observed for the entire dataset. From this finding, we concluded that the number of samples considered for each seasonal subset was high enough for yielding representative site results.

The precision of the measurements influence the results of the trace gas atmospheric variability calculation. The measurement precision for ethane and propane were estimated at ~4% (Pollmann et al., 2008); the precision error was slightly higher for the butane isomers (5% above 100 ppt, ~5 pmol mol^{-1} below 100 ppt). The CO, H_2, and CH_4 measurement precisions were approximately 0.8 ppb, 1.0 ppb, and 0.80 ppb, respectively. The maximum error resulting from these uncertainties on the calculated standard deviations was determined in a Monte-Carlo-style experiment by applying the uncertainty margin of one species on randomly selected measurement values while keeping data for other gases constant. Deviations of the determined variability values were up to 13% from applying the ethane and propane precision error, 21% for the butane isomers, 8% for CO and H_2, and <2% for CH_4.

To fit equation 1 at each site, the variability for the investigated seven compounds was calculated as the standard deviation of natural log-transformed mole fraction ($s_{\ln X}$) for each season for up to five years of data. The atmospheric lifetimes of the six OH-reacting gases were calculated as a function of [OH], according to Equation 2

$$\tau = 1/(k[OH]), \quad (2)$$

using reaction rate constants from Atkinson (1997). A range of [OH] were tested from 5.0×10^4 molecules cm^{-3} to 1.0×10^7 molecules cm^{-3} in increments of 10^3 from 5.0×10^4 to 9.9×10^4 molecules cm^{-3}, increments of 10^4 from 1.0×10^5 to 9.9×10^5 molecules cm^{-3}, and increments of 10^6 from 1.0×10^6 to 1.0×10^7 molecules cm^{-3}. Equation 1 was fitted in MatLab for each site for each season with all 231 possible [OH]. The *A*-value, *b*-value, and [OH] were determined based on the model fit result that yielded the highest coefficient of determination (R^2). The tropospheric lifetime of H_2 was fixed at 700 days based on the average of literature values and was assumed to be invariant across hemispheres and seasons (Hauglustaine and Ehhalt, 2002; Ehhalt and Rohrer, 2009; Yashiro et al., 2011).

2.3. OH results comparisons

The [OH] calculated from equation 2 was compared to model outputs from two sources, i.e. Spivakovsky et al. (2000) and the ECHAM/MESSy Atmospheric Chemistry (EMAC) general circulation model. For the latter, the core atmospheric general circulation model ECHAM5 (Roeckner et al., 2006), interconnected with the Modular Earth Submodel System (MESSy v.2; Jöckel et al., 2010) was used. EMAC submodels represent tropospheric and stratospheric chemistry, radiation, transport and mixing processes, partly mediated by clouds, and describe emissions, atmospheric multiphase chemistry, aerosol and deposition mechanisms (Sander et al., 2005; Jöckel et al., 2006; Kerkweg et al., 2006; Tost et al., 2006, 2007; Pozzer et al., 2010; Brühl et al., 2015). We applied the EMAC model at T42/L31 spatial resolution, i.e., at a spherical spectral truncation of T42 and a quadratic Gaussian grid spacing of about 2.8 degrees latitude and longitude, and 31 hybrid terrain following pressure levels up to 10 hPa. Results have been evaluated against observations (Pozzer et al., 2010, 2012; Christoudias and Lelieveld, 2013; Elshorbany et al., 2014).

3. Results and discussion

3.1. Variability analysis and site characterization

Results for the variability-lifetime relationship vaiables, i.e., *b*-value, *A*-value, and the R^2 for each station for each season, are included in Table 1. All sampled stations display a distinct relationship between atmospheric variability and lifetime. The high R^2-value results from the regression analyses (typically > 0.9) indicate a strong relationship between atmospheric variability and lifetime, similar to findings from previous studies (Jobson et al., 1998, 1999). Our results expand upon these earlier studies, illustrating that the variability-lifetime relationship yields consistent results over a wide latitudinal and temporal range. Variability-lifetime relationship results for five years of June to August data are shown in Figure 2 for four sites that span the globe from north to south. For the more reactive gases there is up to an order of magnitude difference in the gas atmospheric lifetimes between Alert and Hohenpeissenberg. The regression slopes illustrate the consistency and year-to-year variability in the absolute magnitude of the calculated lifetime and variability, and of A- and b-value results within a site. In general, there is a greater difference among sites than between years at a given site.

The median R^2 for both seasons across all sites is 0.91 and the median *b*-value is 0.67. In general, there is a positive correlation between R^2 and b-values ($r=0.53$, $p < 0.0001$), which confirms that the correlation between the lifetime and variability in the atmospheric concentration of a trace gas increases at increasingly remote sites. Figure 3 depicts the latitudinal distribution of the calculated b-values for both seasons. The *b*-values tended to be lower for sites between 30 and 60° N, with the lowest mean annual *b*-value (0.45) at Ochsenkopf and Hohenpeissenberg, both located in mid-continental Germany. The *b*-values > 0.6, indicative of greater 'remoteness', were calculated mostly for remote oceanic and SH sites. Divided by hemisphere, the median *b*-value for December to February is 0.61 for the NH and 0.74 for the SH, and for June to August it is 0.71 for the NH, and 0.78 for the SH. The consistently higher b-values in the SH likely reflect the

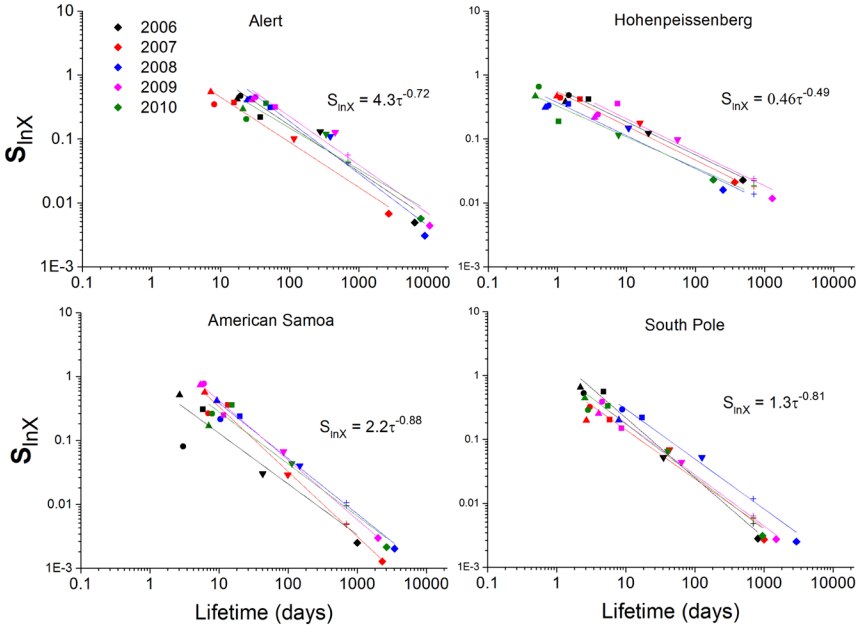

Figure 2

Examples of lifetime-variability plots for 5 years (2006–2010) of June through August data for Alert (82.45° N), Hohenpeissenberg (47.80° N), American Samoa (-14.25° S), and South Pole (-89.98° S).

The plotted lifetime is the best fit result of the variability-lifetime calculations as described in the text for each gas and for each year for each site. The relative order of the lifetime increases was always butanes, propane, ethane, carbon monoxide, and methane. The lifetime of H_2 was fixed at 700 days. Data and the major axis regression line are color-coded for each year. There is a unique symbol for each gas: methane=diamond, H_2=cross, propane=square, *i*-butane = circle, *n*-butane=up triangle, carbon monoxide=down triangle. Equations shown in each graph are the best fit major axis regression including all years of data. Some H_2 data points are on top of each other and are not visible for every year.

doi: 10.12952/journal.elementa.000128.f002

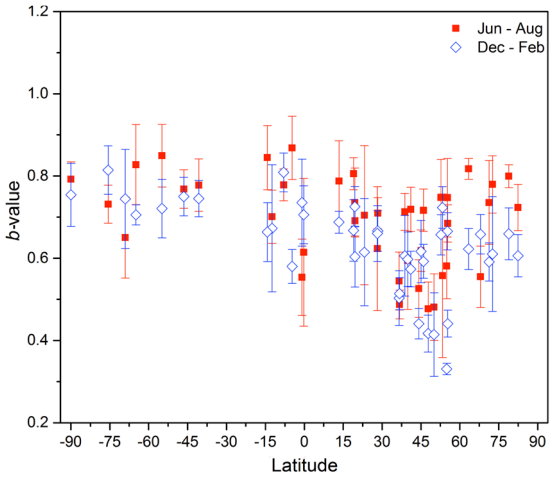

Figure 3

Latitudinal distribution of seasonally averaged *b*-values.

Error bars represent the 1-sigma standard deviation for the data from all the years at each site.

doi: 10.12952/journal.elementa.000128.f003

latitudinal distribution of emissions, which are highest in the temperate northern latitudes between 30° and 60° N. The median annual *b*-value of 0.67 for all sites determined in this work is significantly higher than the *b*-value of 0.5 reported by Jobson et al. (1998, 1999) for background stations. The highest *b*-values (> 0.83) all occur at remote SH sites during June-August and are approaching the b-values of ~1 that were found for stratospheric data sets (Jobson et al., 1999). This similarity suggests that these SH network sites receive extensively processed, photochemically-aged air masses.

Particularly interesting is the observation that the *b*-value in the NH is, for essentially all sites, higher during June to August than during December to February. This suggests that during the NH winter, when OH-dependent lifetimes are longer, these sites are more strongly affected by polluted air, likely from more distant sources, since pollutants are not being removed as effectively from the atmosphere. In the SH, no clear trend is visible; however, as already stated, the SH has lower emissions and network sites on average have a more remote character than those in the NH (SH sites are typically less frequently impacted by short/medium range pollution transport). The sampled air is generally well-processed by the time it reaches the sampling facility, leading to all sites, but one, in both seasons having b-values > 0.6.

Carbon monoxide is a commonly used tracer for anthropogenic pollution as it is formed from incomplete combustion of fossil and biofuels. It would be expected that very remote sites would have little impact from CO pollution, whereas less remote sites (e.g., those with greater influence from anthropogenic emissions) would experience greater variability in atmospheric CO. To further assess the *b*-value as a metric for remoteness, we compared *b*-values for each site with the variability in CO mole fraction. The CO variability was determined from results of the CO analyses of the flask samples, and was calculated as the standard deviation of detrended data (i.e., residuals). While there are differences among seasons and hemispheres (Figure 4),

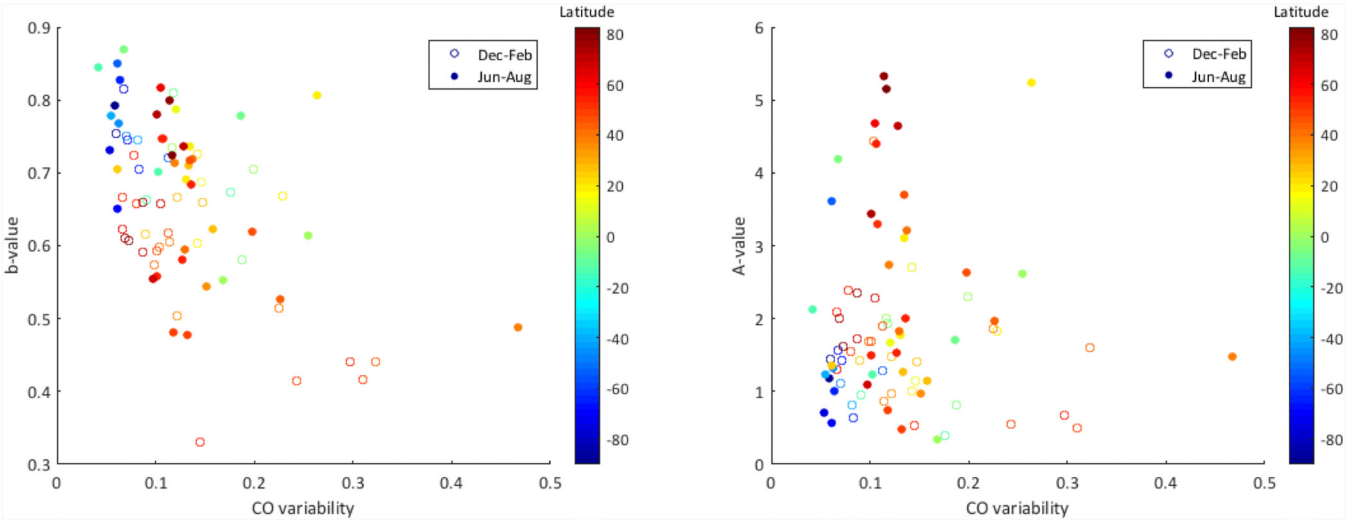

Figure 4

Dependency of the calculated *b*-values (left) and A-values (right) on the variability in atmospheric CO for December–February and June–August color-coded by latitude.

Each point represents an average per season over the years of available data.

doi: 10.12952/journal.elementa.000128.f004

overall there is a negative correlation between the *b*-value and CO variability ($r = -0.52$, $p < 0.0001$). This general relationship of smaller b-values with higher CO variability suggests that the *b*-value is indeed a good indicator of the remoteness of individual sampling sites.

No conclusive explanation for the *A*-value has yet been provided in the literature. In Figure 5, we show the latitudinal and summer-winter distribution of the multi-year seasonally averaged *A*-values. Both the A-value and the seasonal difference in A-values are higher in the NH than the SH. The median *A*-value for December to February is 1.61 for the NH and 1.29 for the SH; for June to August the median A-value is 1.98 for the NH and 1.23 for the SH. Overall, there is a statistically significant positive correlation between the A-values and b-values ($r = 0.48$, $p < 0.0001$; Figure 6). It was previously suggested, based upon the variability-lifetime relationships from other sites, that the *A*-value can be interpreted as a factor that characterizes the range of air mass ages sampled at a site (Williams et al., 2000; Karl et al., 2001), with higher *A*-values indicating a larger range of processed emissions. Unlike the b-values, the A-values, did not have a clear relationship with the variability in CO from long range transport and lower *A*-values representing relatively fresh emissions from closer sources. According to these classifications one would have expected higher *A*-values for the SH sites and in the summer data. The results in Figure 5 show that this assumption mostly holds for the seasonal trend in the data, particularly in the NH; however, our data, with *A*-values of overall similar magnitude in the NH and SH (particularity in the winter), do not show the expected latitudinal behavior based on this interpretation, which would predict higher *A*-values due to a wider spread of emission sources in the SH.

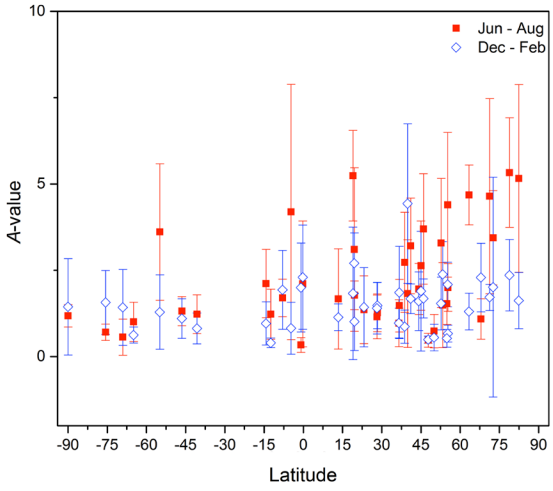

Figure 5
Latitudinal distribution of seasonally averaged *A*-values.

Symbols represent means and error bars represent ± 1 standard deviation of all the years of data.

doi: 10.12952/journal.elementa.000128.f005

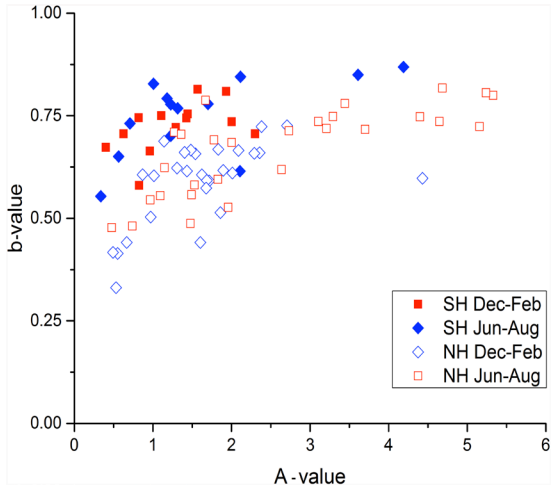

Figure 6
Relationship between A- and b-values.

A-value and b-value results from regression analyses as shown in Figure 2 differentiated by hemisphere and season.

doi: 10.12952/journal.elementa.000128.f006

3.2. Estimation of regional [OH]

Data from all sites display a clear relationship between atmospheric lifetime and variability as documented by the data in Figure 2, yielding typical R^2 linear regression results of > 0.9 (Table 2). From that we concluded that the validity of the variability-lifetime relationship is was sufficient to investigate average [OH] results from the gas variability data. Results of the mean [OH] determined from the variability-lifetime relationship as described in the methods section for both seasons and all sites are summarized in Table 2 and

Table 2. Mean seasonal [OH] (in molecules cm^{-3} x 10^6) calculated from the best fit of the variability-lifetime relationship for the years 2006–2011 (Equation 1)[a]

Station	Code	Latitude	R^2	[OH] Jun – Aug (x 10^6)	[OH] Dec – Feb (x 10^6)
Alert, Canada	ALT	82.45	0.92	0.31 *(0.21)*	0.38 *(0.09)*
Ny Alesund, Norway	ZEP	78.90	0.94	0.48 *(0.16)*	0.37 *(0.14)*
Summit, Greenland	SUM	72.58	0.92	0.61 *(0.15)*	0.41 *(0.08)*
Barrow, AK, USA	BRW	71.32	0.93	0.50 *(0.28)*	0.45 *(0.36)*
Pallas, Finland	PAL	67.97	0.90	1.2 *(0.68)*	0.62 *(0.25)*
Vestmannaeyjar, Iceland	ICE	63.34	0.95	0.63 *(0.30)*	0.54 *(0.19)*
Baltic Sea, Poland	BAL	55.35	0.90	1.7 *(0.85)*	2.3 *(1.4)*
Cold Bay, AK, USA	CBA	55.12	0.95	0.79 *(0.34)*	0.33 *(0.09)*
Lac La Biche, Alberta, Canada	LLB	54.95	0.94	1.4 *(1.0)*	6.0 *(5.7)*
Mace Head, Ireland	MHD	53.33	0.81	0.89 *(0.57)*	0.58 *(0.18)*
Shemya, AK, USA	SHM	52.72	0.94	0.88 *(0.46)*	0.78 *(0.77)*
Ochsenkopf, Germany	OXK	50.06	0.77	3.0 *(4.0)*	5.5 *(4.2)*
Hohenpeissenberg, Germany	HPB	47.80	0.90	5.4 *(3.3)*	6.0 *(2.5)*
Park Falls, WI, USA	LEF	45.93	0.95	0.80 *(0.38)*	0.87 *(0.41)*
Argyle, ME, USA	AMT	45.03	0.88	1.1 *(0.41)*	0.91 *(0.44)*
Black Sea, Romania	BSC	44.17	0.83	0.84 *(0.58)*	0.68 *(0.47)*
Trinidad Head, CA, USA	THD	41.05	0.92	0.88 *(0.34)*	0.30 *(0.13)*
Wendover, UT, USA	UTA	39.90	0.91	1.3 *(0.78)*	0.17 *(0.10)*
The Azores	AZR	38.77	0.90	1.2 *(0.35)*	2.0 *(0.52)*
Southern Great Plains, OK, USA	SGP	36.80	0.89	3.6 *(1.3)*	3.6 (0.60)
Tae-ahn Peninsula, South Korea	TAP	36.73	0.79	3.0 *(2.4)*	0.31 *(0.22)*
Izana, Tennerife	IZO	28.30	0.93	2.5 *(1.0)*	1.7 *(0.85)*
Midway Island	MID	28.21	0.86	2.3 *(1.1)*	2.1 *(1.0)*
Assekrem, Algeria	ASK	23.18	0.85	1.3 *(0.49)*	1.1 *(0.55)*
Mauna Loa, HI, USA	MLO	19.54	0.88	0.98 *(0.43)*	2.6 *(1.4)*
Cape Kumukahi, HI, USA	KUM	19.52	0.94	1.1 *(0.30)*	1.1 *(0.29)*
High Alt. Obs. Ctr, Mexico	MEX	18.98	0.82	0.79 *(0.59)*	3.9 *(5.3)*
Guam	GMI	13.43	0.93	2.4 *(1.2)*	3.1 *(1.8)*
Mount Kenya, Kenya	MKN	-0.05	0.81	6.4 *(3.9)*	1.3 *(0.60)*
Bukit Kototabang, Indonesia	BKT	-0.20	0.89	2.8 *(1.9)*	2.4 *(1.2)*
Seychelles	SEY	-4.67	0.95	1.2 *(0.81)*	5.6 *(3.4)*
Ascension Island	ASC	-7.92	0.91	1.5 *(0.32)*	2.1 *(1.6)*
Arembepe, Bahia, Brazil	ABP	-12.77	0.89	1.0 *(0.67)*	6.4 *(3.1)*
American Samoa	SMO	-14.24	0.91	0.94 *(0.50)*	3.6 *(3.2)*
Cape Grim, Australia	CGO	-40.68	0.92	1.8 *(1.6)*	3.8 *(2.9)*
Crozet Islands	CRZ	-46.45	0.93	1.3 *(0.58)*	2.2 *(1.4)*
Tierra del Fuego, Argentina	TDF	-54.87	0.91	0.78 *(0.34)*	2.5 *(1.3)*
Palmer Station, Antarctica	PSA	-64.92	0.93	1.8 *(0.29)*	3.6 *(2.2)*
Syowa Station, Antarctica	SYO	-69.00	0.88	3.0 *(1.9)*	1.8 *(0.56)*
Halley Station, Antarctica	HBA	-75.58	0.95	1.7 *(0.40)*	2.0 *(0.98)*
South Pole, Antarctica	SPO	-89.98	0.92	1.7 *(0.63)*	2.1 *(1.1)*

[a]The mean R^2 for the variability-lifetime regression is also shown. Values in parentheses represent the 1-σ standard deviation.

doi: 10.12952/journal.elementa.000128.t002

Figure 7. We also plot for comparison the average seasonal [OH] 10-degreee zonal averages for the 200–1000 hPa column based on the model by Spivakovsky et al. (2000) and results for three altitudes from the EMAC model. We chose different altitude ranges to reflect the elevation range in which air is transported to network sites (network sites are spread over an altitude range from sea level to ~4500 m asl). Caution should be exercised in this comparison. As mentioned above, the model outputs are zonal averages, and therefore do not consider particular conditions at the site. Regardless of these constraints, the model representation provides a valuable indication of the latitudinal and seasonal features that are expected to influence [OH] results from the lifetime-variability calculations.

The highest [OH], approximately 6.4 x 10^6 molecules cm^{-3}, was calculated from the flask data for stations near the equator: Mount Kenya (-0.05° S) for June-August, and Arembepe, Brazil, (-12.77° S) for December to February. [OH] decreases towards the high northern and southern latitudes as is expected from lower OH production rates due to decreasing UV insolation and atmospheric [H_2O] moving from the equator towards the poles.

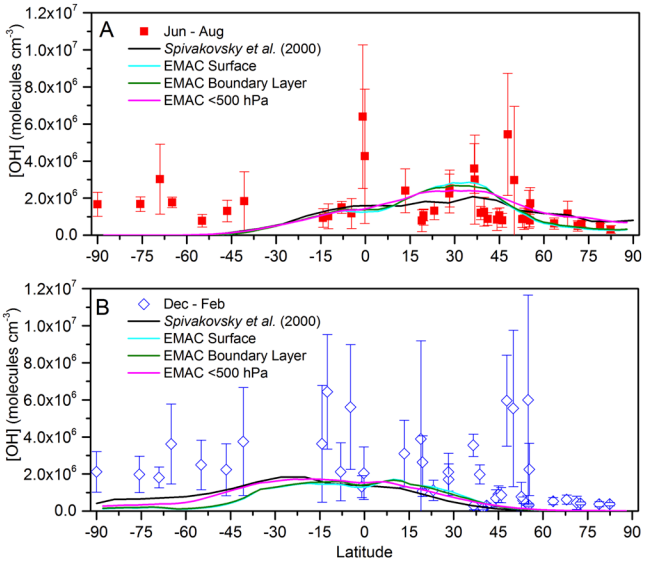

Figure 7

Variability-lifetime derived seasonal mean atmospheric OH concentration, in molecules cm^{-3}, for June through August (top) and December through February (bottom).

Markers represent the mean value for each site from five seasonal analyses each, with error bars representing the 1-sigma standard deviation about the mean. Calculated [OH] are compared to modeled OH latitudinal distribution as calculated with EMAC for June-August and December–February, and results by Spivakovsky et al. (2000) for July and January, respectively.

doi: 10.12952/journal.elementa.000128.f007

Some data from stations located near industrialized mid-northern latitude regions were calculated to have relatively high [OH], with values near 6 x 10^6 molecules cm^{-3}, such as for Lac La Biche, Alberta, and Hohenpeissenberg and Ochsenkopf in Germany. Potentially, rapid conversion of HO_2 to OH due to high NO concentrations in areas with greater anthropogenic pollution can cause these higher OH values as has been previously shown in measurements impacted by outflow from the Los Angeles, CA, metropolitan area (George et al., 1999).

In general, December–February [OH] derived from the variability-lifetime relationship was higher than the modeled [OH], although the latitudinal distribution does reflect the expected low concentrations for the Arctic in the winter and higher [OH] in the Tropics. The EMAC model and the Spivakovsky et al. (2000) model predict [OH] < 1 x 10^5 molecules cm^{-3} for each hemisphere in the winter months at latitudes > 50°, notably lower than the results from the variability-lifetime relationship. Furthermore, the variability-lifetime results for the Antarctic sites during the austral summer (December–February) are remarkably higher than the model output. There have been a number of recent studies that have pointed towards higher wintertime OH production and concentrations than what would be expected from gas phase OH production due to O_3 photolysis alone. These [OH] enhancements have been associated with previously unrecognized heterogeneous photochemistry on snow (Grannas et al., 2007), increased radiation from upwelling light due to the high albedo of snow-covered ground, as well as the reduced mixing over cold surfaces in the winter, which facilitates buildup of surface emissions near the surface. For instance, recent research has shown that nitric oxide (NO) emissions from sunlit snow can cause enhanced NO in the shallow surface layer that develops over snow on the polar snowpack (Davis et al., 2001, 2004, 2008; Helmig et al., 2008b; Neff et al., 2008), leading to enhanced [OH] (Mauldin et al., 2004) and ozone production (Helmig et al., 2008a). Possibly, the [OH] results from the lifetime-variability calculations reflect these [OH] enhancements.

There is a paucity of in-situ OH measurements with which our [OH] estimates from the variability-lifetime analysis can be compared, and when considering only co-located measurements (e.g., measurements conducted at GGGRN sites), there are even fewer. In Table 3, we compare available in-situ 24-hour mean OH observations from six campaigns conducted at network sites for which we have calculated regional [OH] from the variability-lifetime relationship. In most cases, our estimates based on the variability-lifetime relationship are remarkably close to the in-situ measurements, ranging from almost identical at Mace Head to 3.6 times higher at Palmer Station. When one considers the uncertainty associated with in-situ OH measurements (typically ± 50%), most of the measurements and our calculated [OH] estimates can be considered to be within the combined uncertainty windows of both measurements. The tendency that the site specific comparisons appear to yield better agreement than comparison with the model results can also be an indication that the zonal average model [OH] cannot be expected to account for site specific atmospheric chemistry conditions. At lower latitudes differences between the model output and the variability-lifetime relationship at the network sites could be due to local variability in emission sources.

A large year-to-year variability of [OH] results from the variability-lifetime calculations is evident from the error bars added to the medians in Figure 7. This variability by far exceeds the year-to-year changes in [OH] of approximately < ±2.5% that have been estimated in other studies (Rohrer and Berresheim, 2006; Montzka et al., 2011). This points towards low precision and high uncertainty in the [OH] results obtained by the lifetime-variability method. The chemical composition and other controlling factors can be quite different among individual measurement sites, depending on specific local or regional emissions sources

Table 3. Comparison of in-situ [OH] measurements conducted at NOAA Global Greenhouse Gas Reference Network sites with [OH] calculated in this work using the variability-lifetime relationship[a]

OH Measurement Site	Calculated [OH] from this work	24 h-average [OH] from cited literature	Literature Reference
	molecules cm^{-3}	molecules cm^{-3}	
Summit, Greenland Summer 2003	6.1 (1.5) x 10^5	6.4 x 10^6	(Sjostedt et al., 2007)
Summit, Greenland Summer 2008	6.1 (1.5) x 10^5	4.1 x 10^6	(Liao et al., 2011)
Mace Head, Ireland Summer 2002	8.9 *(5.7)* x 10^5	9.1 x 10^5	(Smith et al., 2006)
Hohenpeissenberg, Germany June 2000	5.4 *(3.3)* x 10^6	2 x 10^6	(Handisides et al., 2003)
Izana, Tenerife May 1995	2.5 *(1.0)* x 10^6	2 (0.5) x 10^6	(Armerding et al., 1997)
Cape Grim, Australia February 1999	3.8 *(2.9)* x 10^6	1 x 10^6	(Creasey et al., 2003)
Palmer Station, Antarctica February 1994	3.6 *(2.2)* x 10^6	1.1 x 10^6	(Jefferson et al., 1998)
South Pole, Antarctica Nov-Dec 2000	2.1 *(1.1)* x 10^6	(2.5 – 3.5) x 10^6	(Mauldin et al., 2004)

[a]OH concentrations are expressed in molecules cm^{-3}. Values in parentheses represent the stated uncertainty in the reference study, respectively the 1-σ standard deviation about the mean in the results determined in this study.

doi: 10.12952/journal.elementa.000128.t003

and meteorological conditions. At many of the sites investigated here, the variability-lifetime method does not reproduce the 'expected' seasonal cycle, and gives lower [OH] for the summer and higher [OH] for the winter, especially in the SH. In short, the many factors affecting a particular measurement station must be considered to generate an accurate prediction of [OH], as the 'expected' seasonal cycle may be overwhelmed by either chemical or meteorological impacts. The data used for this analysis were derived from surface measurements, which, in particular in the winter and over snow-covered ground, are from within a shallow boundary layer in which surface emissions accumulate and become determinants in oxidation chemistry. On the other hand, lifetimes of gas species considered in the variability analyses are in excess of days to weeks, which implies [OH] results from the variability-lifetime relationship are also influenced by chemical processing that occurs upwind on regional to hemispheric scales.

4. Summary and conclusions

In this work we applied the atmospheric variability-lifetime relationship to an extensive suite of atmospheric constituents spanning 41 sites world-wide with over 5 years of data to (1) evaluate the applicability of *A*- and *b*-value results for site characterization and (2) to estimate seasonally averaged [OH] on a large regional scale. NH sites in the summer generally had lower b-values, lower A-values, greater variability in [CO], and higher [OH]. We find that this relationship has the potential for evaluating the suitability of sites for background atmospheric measurements based upon the calculated *A*- and *b*-values. Further, our calculations produced [OH] that were of similar magnitude, and in many cases within a factor of two or less of both modeled and measured values. However, variability-derived [OH] does not seem sufficiently accurate to constrain model calculated [OH], as seasonal and meridional contrasts seem to be underestimated. Coordinated studies including simultaneous OH, VOC, and other trace gas measurements would be required for better definition of the comparability and agreement between these methods for [OH] determination. This analysis builds on the first years (2004–2011) of data from the NOAA-INSTAAR global VOC monitoring. This program has since been operating for another five years, extending these data to a more than ten years record. Analytical uncertainties (both precision and accuracy errors) have been steadily reduced over this period and a few additional sites have been added. This opens the possibility to revisit and further expand upon the analyses and findings presented in this paper based on the now available extended data set.

References

Armerding W, Comes FJ, Crawack HJ, Forberich O, Gold G, et al. 1997. Testing the daytime oxidizing capacity of the troposphere: 1994 OH field campaign at the Izaña observatory, Tenerife. *J Geophys Res-Atmos* **102**(D9): 10603–10611. doi: 10.1029/96jd03714.

Atkinson R. 1997. Gas-Phase Tropospheric Chemistry of Volatile Organic Compounds: 1. Alkanes and Alkenes. *J Phys Chem Ref Data* **26**(2): 215–290. doi: 10.1063/1.556012.

Bartenbach S, Williams J, Plass-Dülmer C, Berresheim H, Lelieveld J. 2007. In-situ measurement of reactive hydrocarbons at Hohenpeissenberg with comprehensive two-dimensional gas chromatography (GC×GC-FID): use in estimating HO and NO_3. *Atmos Chem Phys* **7**(1): 1–14. doi: 10.5194/acp-7-1-2007.

Brühl C, Lelieveld J, Tost H, Höpfner M, Glatthor N. 2015. Stratospheric sulfur and its implications for radiative forcing simulated by the chemistry climate model EMAC. *J Geophys Res-Atmos* **120**(5): 2103–2118. doi: 10.1002/2014jd022430.

Christoudias T, Lelieveld J. 2013. Modelling the global atmospheric transport and deposition of radionuclides from the Fukushima Dai-ichi nuclear accident. *Atmos Chem Phys* **13**(3): 1425–1438. doi: 10.5194/acp-13-1425-2013.

Conway TJ, Tans PP, Waterman LS, Thoning KW, Kitzis DR, et al. 1994. Evidence for interannual variability of the carbon cycle from the National Oceanic and Atmospheric Administration/Climate Monitoring and Diagnostics Laboratory Global Air Sampling Network. *J Geophys Res-Atmos* **99**(D11): 22831–22855. doi: 10.1029/94jd01951.

Creasey DJ, Evans GE, Heard DE, Lee JD. 2003. Measurements of OH and HO_2 concentrations in the Southern Ocean marine boundary layer. *J Geophys Res-Atmos* **108**(D15). doi: 10.1029/2002jd003206.

Davis D, Chen G, Buhr M, Crawford J, Lenschow D, et al. 2004. South Pole NO_x chemistry: An assessment of factors controlling variability and absolute levels. *Atmos Environ* **38**(32): 5375–5388.

Davis D, Nowak JB, Chen G, Buhr M, Arimoto R, et al. 2001. Unexpected high levels of NO observed at South Pole. *Geophys Res Lett* **28**(19): 3625–3628.

Davis DD, Seelig J, Huey G, Crawford J, Chen G, et al. 2008. A reassessment of Antarctic plateau reactive nitrogen based on ANTCI 2003 airborne and ground based measurements. *Atmos Environ* **42**(12): 2831–2848.

Dlugokencky EJ, Masaire KA, Lang PM, Tans PP, Steele LP, et al. 1994. A dramatic decrease in the growth rate of atmospheric methane in the northern hemisphere during 1992. *Geophys Res Lett* **21**(1): 45–48. doi: 10.1029/93gl03070.

Ehhalt DH, Rohrer F. 2009. The tropospheric cycle of H_2: A critical review. *Tellus B* **61**(3): 500–535. doi: 10.1111/j.1600-0889.2009.00416.x.

Ehhalt DH, Rohrer F, Wahner A, Prather MJ, Blake DR. 1998. On the use of hydrocarbons for the determination of tropospheric OH concentrations. *J Geophys Res-Atmos* **103**(D15): 18981–18997.

Elshorbany YF, Crutzen PJ, Steil B, Pozzer A, Tost H, et al. 2014. Global and regional impacts of HONO on the chemical composition of clouds and aerosols. *Atmos Chem Phys* **14**(3): 1167–1184. doi: 10.5194/acp-14-1167-2014.

Emmons LK, Arnold SR, Monks SA, Huijnen V, Tilmes S, et al. 2014. The POLARCAT Model Intercomparison Project (POLMIP): Overview and evaluation with observations. *Atmos Chem Phys Discuss* **14**(21): 29331–29393. doi: 10.5194/acpd-14-29331-2014.

Forster P, Ramaswamy V, Artaxo P, Berntsen T, Betts R, et al. 2007. Changes in Atmospheric Constituents and in Radiative Forcing, in, *Climate Change 2007, The Physical Science Basis. Contribution of Working Group I to the Fourth Assessment Report of the Intergovernmental Panel on Climate Change*. Cambridge, UK and New York, NY, USA: Cambridge University Press.

George LA, Hard TM, O'Brien RJ. 1999. Measurement of free radicals OH and HO_2 in Los Angeles smog. *J Geophys Res-Atmos* **104**(D9): 11643–11655. doi: 10.1029/1998jd100113.

Grannas AM, Jones AE, Dibb J, Ammann M, Anastasio C, et al. 2007. An overview of snow photochemistry: Evidence, mechanisms and impacts. *Atmos Chem Phys* **7**(16): 4329–4373. doi: 10.5194/acp-7-4329-2007.

Handisides GM, Plass-Dülmer C, Gilge S, Bingemer H, Berresheim H. 2003. Hohenpeissenberg Photochemical Experiment (HOPE 2000): Measurements and photostationary state calculations of OH and peroxy radicals. *Atmos Chem Phys* **3**(5): 1565–1588. doi: 10.5194/acp-3-1565-2003.

Hauglustaine DA, Ehhalt DH. 2002. A three-dimensional model of molecular hydrogen in the troposphere. *J Geophys Res-Atmos* **107**(D17): ACH 4-1–ACH 4-16. doi: 10.1029/2001jd001156.

Helmig D, Bottenheim J, Galbally IE, Lewis A, Milton MJT, et al. 2009. Volatile organic compounds in the global atmosphere. *Eos Trans AGU* **90**(52).

Helmig D, Johnson B, Oltmans SJ, Neff W, Eisele F, et al. 2008a. Elevated ozone in the boundary layer at South Pole. *Atmos Environ* **42**(12): 2788–2803. doi: 10.1016/j.atmosenv.2006.12.032.

Helmig D, Johnson BJ, Warshawsky M, Morse T, Neff WD, et al. 2008b. Nitric oxide in the boundary-layer at South Pole during the Antarctic Tropospheric Chemistry Investigation (ANTCI). *Atmos Environ* **42**(12): 2817–2830, doi: 10.1016/j.atmosenv.2007.03.061.

Helmig D, Petrenko V, Martinerie P, Witrant E, Rockmann T, et al. 2014. Reconstruction of Northern Hemisphere 1950–2010 atmospheric non-methane hydrocarbons. *Atmos Chem Phys* **14**(3): 1463–1483. doi: 10.5194/acp-14-1463-2014.

Helmig D, Rossabi S, Hueber J, Tans P, Montzka S, et al. 2016. Reversal of global atmospheric ethane and propane trends largely due to US Oil and natural gas production. *Nature Geosci* **9**: 490–495. doi: 10.1038/ngeo2721.

Jefferson A, Tanner DJ, Eisele FL, Davis DD, Chen G, et al. 1998. OH photochemistry and methane sulfonic acid formation in the coastal Antarctic boundary layer. *J Geophys Res-Atmos* **103**(D1): 1647–1656. doi: 10.1029/97jd02376.

Jobson BT, McKeen SA, Parrish DD, Fehsenfeld FC, Blake DR, et al. 1999. Trace gas mixing ratio variability versus lifetime in the troposphere and stratosphere: Observations, *J Geophys Res-Atmos* **104**(D13): 16091–16113. doi: 10.1029/1999jd900126.

Jobson BT, Parrish DD, Goldan P, Kuster W, Fehsenfeld FC, et al. 1998. Spatial and temporal variability of nonmethane hydrocarbon mixing ratios and their relation to photochemical lifetime. *J Geophys Res-Atmos* **103**(D11): 13557–13567.

Jöckel P, Kerkweg A, Pozzer A, Sander R, Tost H, et al. 2010. Development cycle 2 of the Modular Earth Submodel System (MESSy2). *Geosci Model Dev* **3**(2): 717–752. doi: 10.5194/gmd-3-717-2010.

Jöckel P, Tost H, Pozzer A, Bruhl C, Buchholz J, et al. 2006. The atmospheric chemistry general circulation model ECHAM5/MESSy1: Consistent simulation of ozone from the surface to the mesosphere. *Atmos Chem Phys* **6**: 5067–5104.

Junge CE. 1974. Residence time and variability of tropospheric trace gases. *Tellus* **26**(4): 477–488. doi: 10.1111/j.2153-3490.1974.tb01625.x.

Karl T, Crutzen PJ, Mandl M, Staudinger M, Guenther A, et al. 2001. Variability-lifetime relationship of VOCs observed at the Sonnblick Observatory 1999 - estimation of HO-densities. *Atmos Environ* **35**(31): 5287–5300.

Karl T, Guenther A. 2004. Atmospheric variability of biogenic VOCs in the surface layer measured by proton-transfer-reaction mass spectrometry. *Int J Mass Spectrom* **239**(2–3): 77–86. doi: 10.1016/j.ijms.2004.09.023.

Karl T, Guenther A, Spirig C, Hansel A, Fall R. 2003a. Seasonal variation of biogenic VOC emissions above a mixed hardwood forest in northern Michigan. *Geophys Res Lett* **30**(23). doi: 10.1029/2003gl018432.

Karl T, Hansel A, Mark T, Lindinger W, Hoffmann D. 2003b. Trace gas monitoring at the Mauna Loa Baseline observatory using proton-transfer reaction mass spectrometry, *Int J Mass Spectrom* **223**(1–3): 527–538. doi: 10.1016/s1387-3806(02)00874-6.

Kerkweg A, Sander R, Tost H, Jöckel P. 2006. Technical note: Implementation of prescribed (OFFLEM), calculated (ONLEM), and pseudo-emissions (TNUDGE) of chemical species in the Modular Earth Submodel System (MESSy). *Atmos Chem Phys* **6**(11): 3603–3609. doi: 10.5194/acp-6-3603-2006.

Laube LC, Gallacher E, Oran DF, Bonisch H, Engel A, et al. 2015. Atmospheric lifetime implications for SF_6 from stratospheric observations. *InGOS Conference, Utrecht, The Netherlands, 21-24 September*. http://www.ingos-infrastructure.eu/wp-content/uploads/2015/08/InGOS-Conference-Laube-Atmospheric-lifetime-implications-for-SF_6-from-stratospheric-observations.pdf.

Lawson SJ, Selleck PW, Galbally IE, Keywood MD, Harvey MJ, et al. 2015. Seasonal in situ observations of glyoxal and methylglyoxal over the temperate oceans of the Southern Hemisphere. *Atmos Chem Phys* **15**(1): 223–240. doi: 10.5194/acp-15-223-2015.

Liao J, Sihler H, Huey LG, Neuman JA, Tanner DJ, et al. 2011. A comparison of Arctic BrO measurements by chemical ionization mass spectrometry and long path-differential optical absorption spectroscopy. *J Geophys Res-Atmos* **116**. doi: 10.1029/2010jd014788.

Maiss M, Brenninkmeijer CAM. 1998. Atmospheric SF_6: Trends, sources, and prospects. *Environ Sci Technol* **32**(20): 3077–3086. doi: 10.1021/es9802807.

Mauldin RL, Kosciuch E, Henry B, Eisele FL, Shetter R, et al. 2004. Measurements of OH, HO_2+RO_2, H_2SO_4, and MSA at the South Pole during ISCAT 2000. *Atmos Environ* **38**(32): 5423–5437.

Montzka SA, Krol M, Dlugokencky E, Hall B, Jöckel P, et al. 2011. Small Interannual Variability of Global Atmospheric Hydroxyl. *Science* **331**(6013): 67–69. doi: 10.1126/science.1197640.

Neff W, Helmig D, Grachev A, Davis D. 2008. A study of boundary layer behavior associated with high NO concentrations at the South Pole using a minisodar, tethered balloon, and sonic anemometer. *Atmos Environ* **42**(12): 2762–2779.

NOAA. 2016a. ESRL/GMD FTP Data Finder. NOAA Earth Systems Research Laboratory Global Monitoring Division. http://www.esrl.noaa.gov/gmd/dv/data/. Accessed August 2016.

NOAA. 2016b. Curve Fitting Methods Applied to Time Servies in NOAA/ESRL/GMD. NOAA Earth Systems Research Laboratory Global Monitoring Division. http://www.esrl.noaa.gov/gmd/ccgg/mbl/crvfit/crvfit.html. Accessed August 2016.

Plass-Dülmer C, Michl K, Ruf R, Berresheim H. 2002. C_2–C_8 hydrocarbon measurement and quality control procedures at the Global Atmosphere Watch observatory Hohenpeissenberg. *J Chromatogr A* **953**(1–2): 175–197. doi: 10.1016/s0021-9673(02)00128-0.

Pollmann J, Helmig D, Hueber J, Plass-Dülmer C, Tans P. 2008. Sampling, storage, and analysis of C_2-C_7 non-methane hydrocarbons from the US National Oceanic and Atmospheric Administration Cooperative Air Sampling Network glass flasks. *J Chromatogr A* **1188**(2): 75–87.

Pollmann J, Helmig D, Hueber J, Tanner D, Tans PP. 2006. Evaluation of solid adsorbent materials for cryogen-free trapping - gas chromatographic analysis of atmospheric C_2-C_6 non-methane hydrocarbons. *J Chromatogr A* **1134**(1–2): 1–15.

Pozzer A, de Meij A, Pringle KJ, Tost H, Doering UM, et al. 2012. Distributions and regional budgets of aerosols and their precursors simulated with the EMAC chemistry-climate model. *Atmos Chem Phys* **12**(2): 961–987. doi: 10.5194/acp-12-961-2012.

Pozzer A, Pollmann J, Taraborrelli D, Jöckel P, Helmig D, et al. 2010. Observed and simulated global distribution and budget of atmospheric C_2-C_5 alkanes. *Atmos Chem Phys* **10**(9): 4403–4422. doi: 10.5194/acp-10-4403-2010.

Reddmann T, Ruhnke R, Kouker W. 2001. Three-dimensional model simulations of SF_6 with mesospheric chemistry. *J Geophys Res-Atmos* **106**(D13): 14525–14537. doi: 10.1029/2000jd900700.

Rhee TS, Brenninkmeijer CAM, Röckmann T. 2006. The overwhelming role of soils in the global atmospheric hydrogen cycle. *Atmos Chem Phys* **6**(6): 1611–1625. doi: 10.5194/acp-6-1611-2006.

Roeckner E, Brokopf R, Esch M, Giorgetta M, Hagemann S, et al. 2006. Sensitivity of simulated climate to horizontal and vertical resolution in the ECHAM5 atmosphere model. *J Clim* **19**(16): 3771–3791. doi: 10.1175/jcli3824.1.

Rohrer F, Berresheim H. 2006. Strong correlation between levels of tropospheric hydroxyl radicals and solar ultraviolet radiation. *Nature* **442**(7099): 184–187.

Sander R, Kerkweg A, Jöckel P, Lelieveld J. 2005. Technical note: The new comprehensive atmospheric chemistry module MECCA. *Atmos Chem Phys* **5**(2): 445–450. doi: 10.5194/acp-5-445-2005.

Schultz MG, Akimoto H, Bottenheim J, Buchmann B, Galbally IE, et al. 2015. The Global Atmosphere Watch reactive gases measurement network. *Elem Sci Anth* **3**(000067). doi: 10.12952/journal.elementa.000067.

Sjostedt SJ, Huey LG, Tanner DJ, Peischl J, Chen G, et al. 2007. Observations of hydroxyl and the sum of peroxy radicals at Summit, Greenland during summer 2003. *Atmos Environ* **41**(24): 5122–5137. doi: 10.1016/j.atmosenv.2006.06.065.

Smith SC, Lee JD, Bloss WJ, Johnson GP, Ingham T, et al. 2006. Concentrations of OH and HO_2 radicals during NAMBLEX: measurements and steady state analysis. *Atmos Chem Phys* **6**(5): 1435–1453. doi: 10.5194/acp-6-1435-2006.

Spivakovsky CM, Logan JA, Montzka SA, Balkanski YJ, Foreman-Fowler M, et al. 2000. Three-dimensional climatological distribution of tropospheric OH: Update and evaluation. *J Geophys Res-Atmos* **105**(D7): 8931–8980. doi: 10.1029/1999jd901006.

Tanner D, Helmig D, Hueber J, Goldan P. 2006. Gas chromatography system for the automated, unattended, and cryogen-free monitoring of C_2 to C_6 non-methane hydrocarbons in the remote troposphere. *J Chromatogr A* **1111**(1): 76–88. doi: 10.1016/j.chroma.2006.01.100.

Tost H, Jöckel P, Kerkweg A, Pozzer A, Sander R, et al. 2007. Global cloud and precipitation chemistry and wet deposition: Tropospheric model simulations with ECHAM5/MESSy1. *Atmos Chem Phys* **7**(10): 2733–2757: doi: 10.5194/acp-7-2733-2007.

Tost H, Jöckel P, Kerkweg A, Sander R, Lelieveld J. 2006. Technical note: A new comprehensive SCAVenging submodel for global atmospheric chemistry modelling. *Atmos Chem Phys* **6**(3): 565–574. doi: 10.5194/acp-6-565-2006.

WCC-VOC. 2016. World Calibration Centre for Volatile Organic Compounds. Karlsruhe Institute of Technology. http://www.imk-ifu.kit.edu/wcc-voc/. Accessed February 2016.

WDCGG. 2016. World Data Centre for Greenhouse Gases. http://ds.data.jma.go.jp/gmd/wdcgg/. Accessed Oct. 2015.

Williams J, de Reus M, Krejci R, Fischer H, Ström J. 2002. Application of the variability-size relationship to atmospheric aerosol studies: estimating aerosol lifetimes and ages. *Atmos Chem Phys* **2**(2): 133–145. doi: 10.5194/acp-2-133-2002.

Williams J, Fischer H, Harris GW, Crutzen PJ, Hoor P, et al. 2000. Variability-lifetime relationship for organic trace gases: A novel aid to compound identification and estimation of HO concentrations. *J Geophys Res-Atmos* **105**(D16): 20473–20486. doi: 10.1029/2000jd900203.

Williams J, Gros V, Bonsang B, Kazan V. 2001. HO cycle in 1997 and 1998 over the southern Indian Ocean derived from CO, radon, and hydrocarbon measurements made at Amsterdam Island. *J Geophys Res-Atmos* **106**(D12): 12719–12725.

Yashiro H, Sudo K, Yonemura S, Takigawa M. 2011. The impact of soil uptake on the global distribution of molecular hydrogen: Chemical transport model simulation. *Atmos Chem Phys* **11**(13): 6701–6719. doi: 10.5194/acp-11-6701-2011.

Contributions

- Contributed to conception and design: JP, DH, CRT, PPT, JL
- Contributed to acquisition of data: JP, DH, JH, PPT
- Contributed to analysis and interpretation of data: JP, DH, DL, CRT, PPT, JL
- Drafted and revised the article: JP, DH, DL, CRT, PPT, JL
- Approved and submitted version for publication: JP, DH, DL, CRT, JH, PPT, JL

Acknowledgments

Ken Masarie (NOAA-ESRL) helped with the database management. E. Dlugokencky, P. Novelli, P. Lang (all NOAA-ESRL) provided unpublished trace gas data from the NOAA Global Greenhouse Gas Reference Network. Korbinian Hens (MPI) programmed the 2-dimensional routine for the calculation of OH concentrations. The authors thank the personnel at the network sites and the NOAA flask team for their efforts in maintaining the network program.

Funding information

This research was funded through NOAA's Office of Oceanic and Atmospheric Research.

Competing interests

The authors have no competing interests, as defined by Elementa, that might be perceived to influence the research presented in this manuscript.

Data accessibility statement

Data sources are cited in the text of the manuscript with the URL listed in the references.